Received: 8 October 2022 | Accepted: 21 December 2022

DOI: 10.1002/pamm.202200253

Internal prestressing of ultra-high performance concrete using shape memory fibers

Stefan Descher[1,*], **Philipp Krooß**[2], **Detlef Kuhl**[1], **Alexander Wetzel**[3], and **Sebastian Wolf**[1]

[1] Institute of Structural Mechanics, University of Kassel, Mönchebergstr. 7, 34125 Kassel, Germany
[2] Institute of Materials Engineering, Metallic Materials, University of Kassel, Mönchebergstr. 3, 34125 Kassel, Germany
[3] Institute for Structural Materials and Construction Chemistry, University of Kassel, Mönchebergstr. 7, 34125 Kassel, Germany

Using shape memory fibers to reinforce concrete is a novel concept in civil engineering. Pre-stretched fibers are brought into concrete and after activating the shape memory effect, a compressive prestress state is introduced. The present work investigates this method numerically. A brief introduction to the relevant behavior of shape memory alloys is given. Fiber activation is modeled by an empirical phase transition model. Simulations are carried out by applying the Finite Element Method to solve the CAUCHY-FOURIER equations. Results of studies are presented for single-fiber, improved single-fiber and multi-fiber configurations. Special focus is put on the geometric type of strain release. Key findings are that compressive stresses can be introduced into the concrete, however, local tension will occur. By altering the fiber geometry and applying an elastomeric coating, these regions can be eliminated. Furthermore, when using multiple fibers, there are synergies between regions of compression.

1 Introduction

The use of steel fibers to reinforce concrete is a widespread application in civil engineering. The general method to manufacture structures with this material is that a certain volume fraction of fibers (up to 3%, [1]) is included into fresh concrete. Afterwards, the fluid-solid compound is casted into a mold. Curing leads to a solid-solid compound, in which concrete is considered to be the continuous matrix in which fibers are dispersedly embedded. It is well known that thereby, tensile strength, cracking and thermal behavior is influenced positively. However, a coarse matrix that e.g. includes large pores or stones weakens the bond, which limits these capabilities. Consequently, an optimization of the matrix by usage of finer materials, commonly a mixture of cement, quartz powder and silica fume, was promoted. It led to Ultra-High Performance Concrete (UHPC) [2], which stands out because of a dense matrix. It allows to realize comparatively slender and much more durable structures, because the above-named benefits are even greater in this material.

Achievement of further improvement lays in optimizing fibers, which is topic of the present work. There are two approaches highlighted hereafter, which are combined for investigation. The first is to alter fiber geometry. One example is to use deformed fibers [3], which can be considered one of the earlier concepts. More recent works deal with the introduction of end hooks [4]. In any way, an improvement of tensile performance and pull-out behavior can be reached. The second approach addresses fiber material. Novel works propose using smart materials to introduce an internal state of compressive stress. [5] The concept is to use shape memory alloys (SMA), which are known to show the so-called one-way effect. This means, plastic deformations that are brought into the material can be recovered by heating it up. Regarding improvement of UHPC, this means, fibers can be pre-stretched before they are brought into fresh concrete. After curing, their memory effect can be activated, which will cause a compressive stress state inside the structure as a result of fiber contraction. Ideally, both approaches are combined. Even further improvement can be reached by application of an elastomeric coating. [6] A key point is that newly developed, iron-based alloys are used. In comparison to NiTi, which is a popular SMA, they are much cheaper to manufacture, which makes their application realistic in an economical sense. The basic alloy is Fe–Mn–Al–Ni, to which further components are added, see [8]. For heating up the fibers, there are two concepts. The first is to heat up the entire structure. Considering that structures in civil engineering are large, this would require a great amount of energy, since the matrix needs to warm up as well. Consequently, in the second concept, it is intended to heat up the fibers by induction, which allows to reduce the required energy dramatically. For this purpose, a high-frequency electromagnetic field is applied by a coil, see [9].

The present work investigates the final prestress-state for a single fiber, improved single fiber with tip modifications and regular multi-fiber configurations. For the single fiber configuration, a complete thermal activation cycle is investigated to gain information about geometric dependencies in strain release. Induction of thermal energy as well as prestretching of fibers is considered in a simplified manner. The phase transition causing a release of strain is modeled by an empirical function. Focus is to identify and study regions of compression and strain as well as parameters that have an influence.

* Corresponding author: e-mail descher@uni-kassel.de, phone +49 561 804 2698, fax +49 561 804 3631

2 Strain Release Model for Shape Memory Alloys

To create a prestress-state, the one-way effect is made use of. Fig. 1 (left) shows an example of pre-stretching followed by shape recovery. In the present work, it is used to give an overview of transitions that occur in such cycle. The data originates from experiments for NiTi that are presented by HARTL and LAGOUDAS in [10]. State ① represents the virgin material in which the microstructure is twinned martensite. When stretching the material, the microstructure detwins. In the stress-strain curve, this phase transformation manifests as yielding, visible between ① and ②. At the end of this region, towards ②, it is superimposed with elastic behavior, which shows that the martensite is detwinned. After unloading, at point ③, strain is stored and the stress-free state is reached again. It corresponds to the configuration, in which fibers would be included into fresh concrete. Afterwards, the mixture is casted into molds, the concrete is given time to cure, followed by thermal activation of the fibers. Thermal activation corresponds to the process between ③ and ④, where detwinned martensite is transformed into austenite. When cooling down from ④ to ①, austenite is transformed back to twinned martensite, which does not show an influence on the stress and strain levels in the given representation.

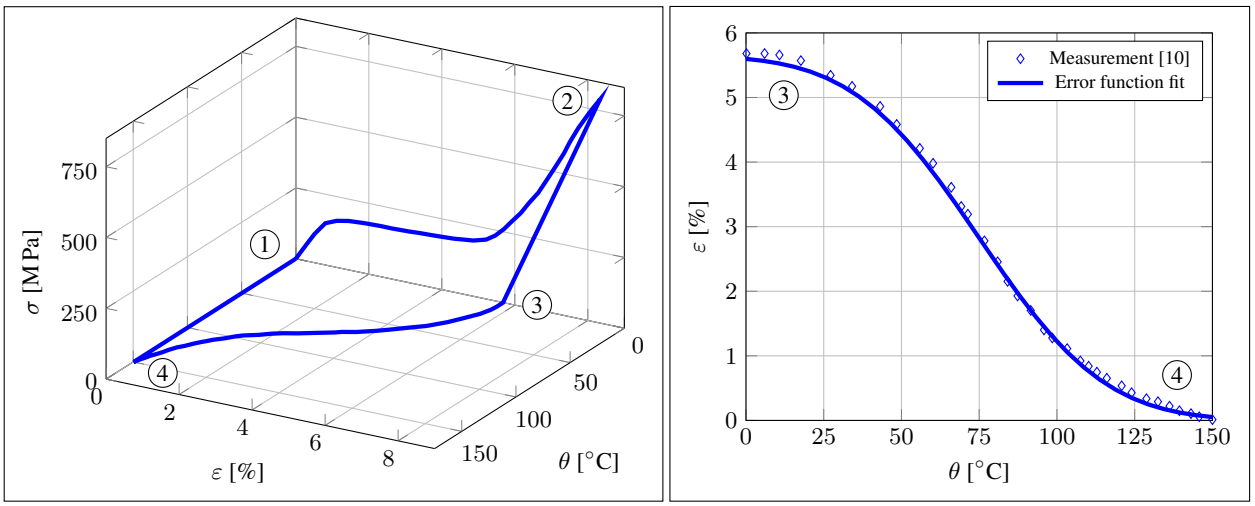

Fig. 1: Left: Stress-strain-temperature curve for Niti as presented by HARTL and LAGOUDAS in [10]. Right: Detailed progress of strain release during heating to which an error function can be fitted with only small deviations.

The present work highlights the prestressing cycle. It corresponds to the curve section ③→④→① of Fig. 1 (left). As determined, only the transformation from detwinned martensite to austenite will influence strain. For this reason, exclusively the phase change between ③ and ④ is modeled. Fig. 1 (right) shows the progress of strain in detail. Considering that change rates in phase transitions often follow a GAUSSIAN bell curve, it is a good practice to model phase transitions with error functions. They result when integrating these curves over time or temperature, depending on the experimental foundation. A work that uses Differential Scanning Calorimetry for investigating SMAs and presents such bell curves over temperature is [11]. That this proceeding works quite well can be seen when comparing the error function fit to experimental data in Fig. 1 (right). On this basis, an empirically motivated phase transition model is defined as follows.

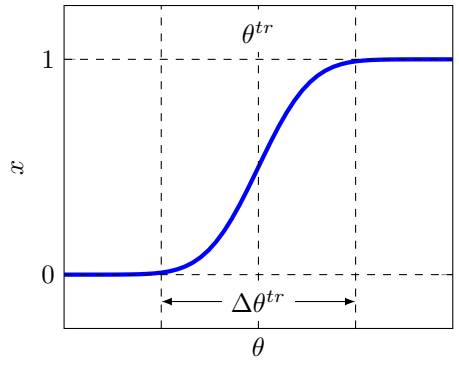

Fig. 2: Parameter interpretation of eq. (1). Detwinned martensite correspond to $x = 0$, austenite to $x = 1$.

An indicator x is introduced to describe the state of strain release. Considering the above-named phase transitions, this means $x = 0$ corresponds to detwinned martensite, $x = 1$ to austenite. For this purpose, an error function is scaled and shifted to describe an increase of x from lower to higher temperatures in these limits. The resulting function

$$x(\theta) = \frac{1}{2}\left[1 - erf\left(\frac{4\sqrt{ln2}(\theta^{tr} - \theta)}{\Delta\theta^{tr}}\right)\right] \tag{1}$$

is characterized by the transition temperature θ^{tr} and the transition temperature range $\Delta\theta^{tr}$. Fig. 2 shows, θ^{tr} is the temperature at which $x = 0.5$, $\Delta\theta^{tr}$ scales the transition region over temperature. Since it is desired to describe a full activation cycle, the condition $\dot{x} > 0$ will be considered. It prevents the transformation strains to decrease in cooling.

To connect phase transformation and strains, a linear dependency of the transformation strain tensor $\boldsymbol{\varepsilon}^{tr}$ on x is suited. It implies that a constitutive model to connect a scalar and tensor of rank two is required. Typical experiments to determine stress-strain-temperature curves, as presented in Fig. 1 (left), are performed with wires though. This means, they are considered one-dimensional and transverse effects are left out. As a result, it is not clear how to link x to the components of $\boldsymbol{\varepsilon}^{tr}$. For that

reason, in the present work, three assumptions are object of study. Firstly, it is considered that the change from detwinned martensite to austenite is a change of crystal structure. For that reason, volumetric release is assumed. Secondly, it is assumed that strain is released uniaxially, dependent on the direction it was brought in. Thirdly, a combination of both, denoted as mixed. For the axisymmetric case, in which the diagonal elements of the stored strain tensor $\boldsymbol{\varepsilon}^0$ are ε^0_{rr}, ε^0_{zz} and $\varepsilon^0_{\phi\phi}$, apart from that ε^0 denoted as level of stored strain, the release equation is

$$\boldsymbol{\varepsilon}^{tr}(\theta) = -\boldsymbol{\varepsilon}^0 x(\theta), \qquad \frac{\boldsymbol{\varepsilon}^0}{\varepsilon^0} = \underbrace{\begin{bmatrix}1&0&0\\0&1&0\\0&0&1\end{bmatrix}}_{\text{volumetric}}, \underbrace{\begin{bmatrix}0&0&0\\0&1&0\\0&0&0\end{bmatrix}}_{\text{uniaxial}}, \underbrace{\begin{bmatrix}\frac{1}{2}&0&0\\0&1&0\\0&0&\frac{1}{2}\end{bmatrix}}_{\text{mixed}}. \tag{2}$$

It enables to consider strain release in a thermomechanical simulation procedure, just as known for thermal strains. Note that only one-way coupling is possible, since stresses are not considered in the equation. Furthermore, energy consumption and release during phase change [12] is neglected. However, there is a possibility to extend the model for endo- and exothermic effects by modeling a source term of the energy equation using $\dot{x}$, see [13].

3 Governing Equations and Numerical Methods

For simulating an inductive heating process, as is intended to use for fiber activation, the MAXWELL equations need to be solved. It is known to be an extensive task, see [14], consequently a simplified method is favored in this early stage of work. It allows studying the general concept of internal prestressing by only solving the CAUCHY-FOURIER equations. Central feature is that alternating electromagnetic fields mainly cause a heat source close to the surface of metallic objects, see [15]. As a result, the energy equation

$$\rho\, c\, \dot{\theta} + \operatorname{div}[-\lambda \operatorname{grad}\theta] = Q \tag{3}$$

contains a source term Q, that is only active in certain regions of the fiber. Furthermore, to consider the temperature cycle for activation, it is switched off after $x = 1$ is reached throughout the fiber. Temperature occurs in the thermal and transition strain term of the constitutive model, that is inserted in the momentum equation

$$\rho\ddot{\mathbf{u}} = \operatorname{div}\boldsymbol{\sigma}, \qquad \boldsymbol{\sigma} = \mathbb{C} : \left[\nabla^{sym}\mathbf{u} - \boldsymbol{\varepsilon}^{\theta}(\theta) - \boldsymbol{\varepsilon}^{tr}(\theta)\right]. \tag{4}$$

Since coupling is one-sided and effects of inertia in the structure are neglectable, it is possible to solve the energy equation in time and adapt the momentum equation to the current temperature field only if results are written out. In the present work, this was realized by application of the NEWMARK-α time integration scheme and the Finite Element Method using biquadratic LAGRANGE-elements. A transient simulation is only carried out to study the interaction of thermal and transition strains. Note by setting $x = 1$ in the fiber region, the final prestress state can be calculated without having to perform a transient simulation.

4 Fiber-Concrete Interaction Studies

To investigate the impact of fibers on their proximity in a realistic way, an axisymmetric model is used. Aim is to identify the capabilities to introduce a compressive stress state and interactions with thermal strain during the activation cycle. Object of study is a conventional fiber, as well as an improved fiber with anchors, that is coated by an elastomer as it is suggested in [6]. Parameters of eq. (1) are set to $\theta^{tr} = 323.15$ K and $\Delta\theta^{tr} = 10$ K, which is the desired range for the newly developed, iron-based SMAs. For realization, a computational domain that is uniformly meshed with a resolution of 10 elements/R is divided in domains as shown in Fig. 3. The corresponding material parameters are documented in Table 1. Note that the thickness of the domains 'SMA w/ heat source' and 'elastomeric coating' is one element and the concrete's surface is cooled to room temperature.

Table 1: Material data and heat source distribution for the domains named in Fig. 3.

Domain	ρ [kg m^{-3}]	c [J kg^{-1} K^{-1}]	λ [W m^{-1} K^{-1}]	Q [W m^{-3}]	E [Pa]	ν [-]	α [-]
SMA w/o heat source	7850	500	50	0	210e+09	0.3	12e-06
SMA w/ heat source	7850	500	50	2.5e+08	210e+09	0.3	12e-06
elastomeric coating	1250	1700	0.2	0	1e+06	0.49	20e-06
concrete	2500	1000	2	0	30e+09	0.2	9e-06

Separation of the SMA fiber into two regions exists to mimic inductive heating. Extensive studies in [16] showed that the penetration depth of JOULE heating in steel depends strongly on the frequency of the electromagnetic field. However, it always is strongest in regions close to the surface. As a result, the outer element layer of the fiber contains a non-zero heat source Q, that is strong enough to activate the entire SMA domain. After 12 seconds, the fiber temperature reaches approximately 60°C. At this point, $Q = 0$ is set, which initiates cooling by the outer boundaries.

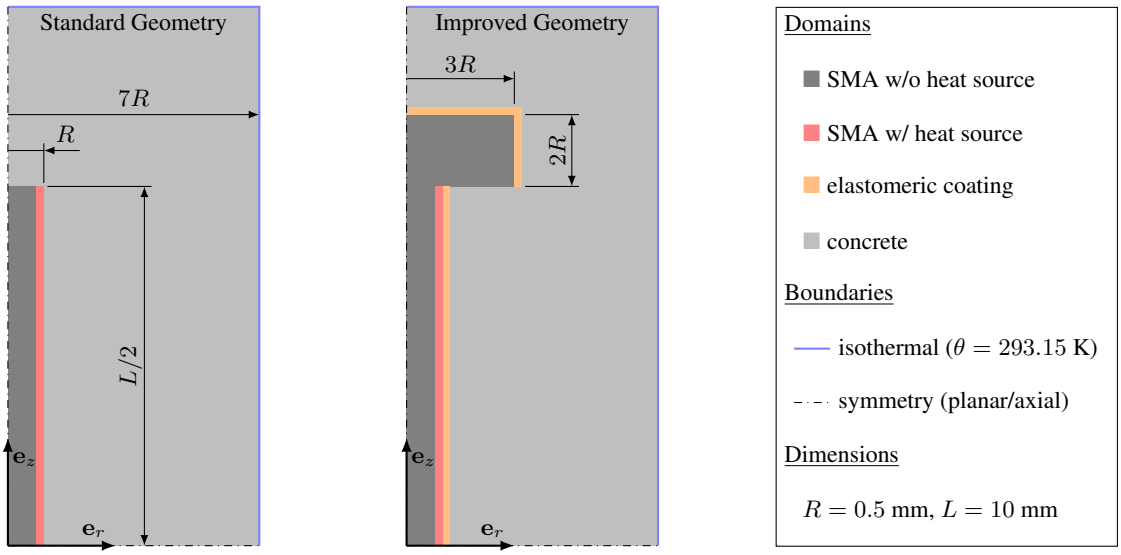

Fig. 3: Case definitions for investigating the standard and improved fiber geometry. The colored domains thickness is one element, the overall resolution is 10 biquadratic LAGRANGE-elements over the fiber radius. A symmetry boundary condition is used at $z = 0$.

Evaluation of the activation process for the standard geometry is done by observing stresses at the concrete side of the interface at $r = R$ and $z = 0$. The top part of Fig. 4 shows that generally, thermal and transition strains counteract each other. Compared to the pre-strain levels applied in Fig. 1, relatively small values of ε^0 already overpower thermal effects. The release of strains already sets in right at the start and is completed at around $t = 4$ s throughout the fiber. Well above that, still minor changes in temperature occur. When cooling is initiated, thermal stresses vanish and the final state of stress is reached. It shows that at the given location, in concrete, fiber contraction leads to radial tension as well as longitudinal and circumferential compression. The upper part's curves correspond to volumetric strain release. How the strain release type influences final values of stress is shown in the lower part of Fig. 4.

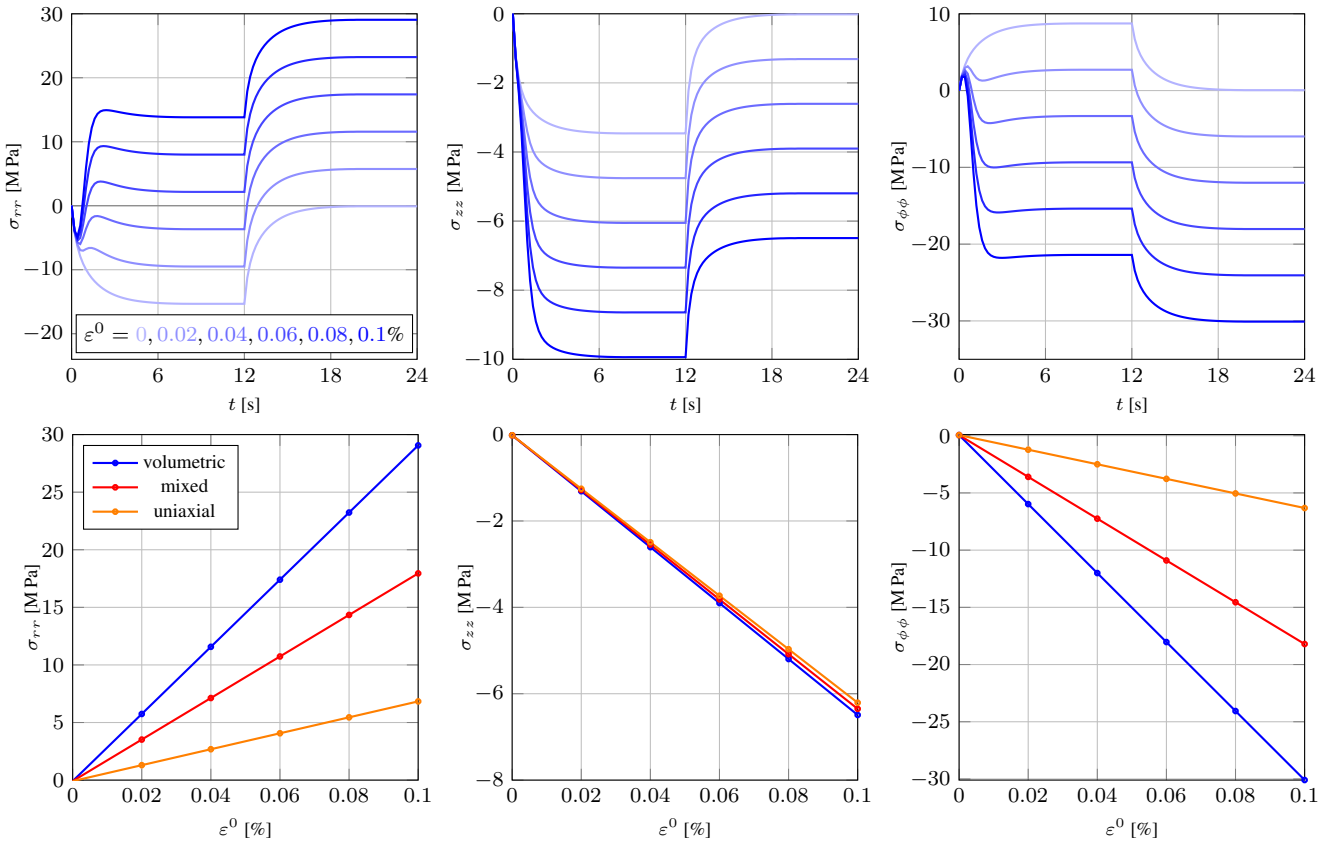

Fig. 4: Activation cycle in the standard geometry. Top: Evaluation of stresses in concrete at $r = R$ and $z = 0$ for volumetric strain release. At $t = 12$ s, the heat source is deactivated. Bottom: Influence of the strain release type on the final stress values.

It shows that radial and circumferential stresses are very sensitive on the strain release type. The occurrence of longitudinal and circumferential compression, as well as radial tension, is independent on it. Regarding that concrete reacts very sensitive to tension, which is also true for the fiber-concrete interface bond, it is important to know that a reduction of strain release normal to the direction of pre-stretching is beneficial. How fiber contraction influences other regions is shown in Fig. 5.

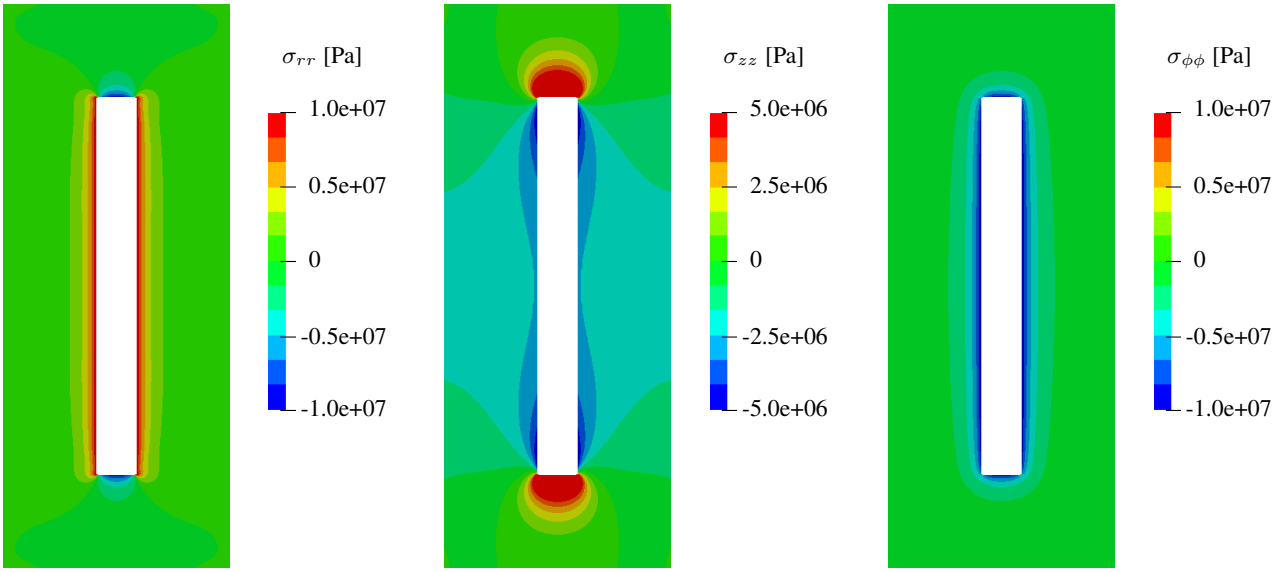

Fig. 5: Final state of stress inside the concrete domain for the standard fiber geometry. Strain is released volumetrically.

It reveals that over the entire fiber length, there is radial tension in concrete. In longitudinal direction, there is compression in radial proximity of the fiber. At its tips, there are pronounced regions of tension. In circumferential direction, exclusively compression occurs. Regarding the magnitude of tension stresses, this leads to the conclusion that the fiber geometry needs to be optimized. Following the design of large construction elements that are commonly used for prestressing of concrete structures, tip anchors were introduced. Furthermore, as described above, an elastomeric coating is introduced. Except the anchors' bottoms, it covers all surfaces, see Fig. 3 (center).

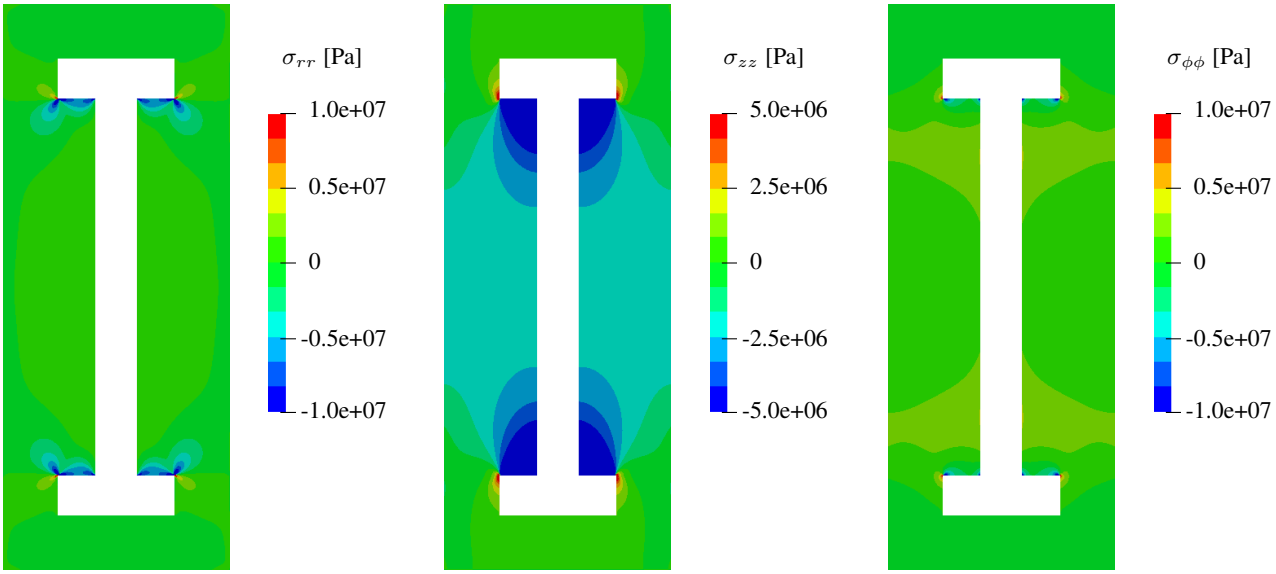

Fig. 6: Final state of stress inside the concrete domain for the improved fiber geometry. Strain is released volumetrically.

Fig. 6 shows that this proceeding eliminates all critical regions of tension. Still, at geometric singularities, there are peaks. However, there is doubt that they occur in a real geometry. Compared to the straight fiber, longitudinal compression could be improved, circumferential compression vanishes though. If an elastomeric coating is needed might seem arguable since the fiber-concrete bond might get lost in regions of tension anyway. However, another benefit discovered, but not depicted, is that the elastomeric coating thermally insulates the fiber. As a result, much smaller values of Q were needed to heat it up to 60°C. Regarding that electromagnetic fields drop strongly in distance to a coil [17], it increases the range of activatability, which is valuable. Furthermore, it improves pull-out behavior, which is experimentally proven in [6, 7].

In a realistic geometry, fibers are oriented randomly to each other. However, in some regions, they are aligned, see [18]. It is motivation for the multi-fiber study presented in Fig. 7. Here, horizontal and vertical spacing is $L/2$ and simulations were carried out for plane stress with the previously described resolution of 10 elements/R.

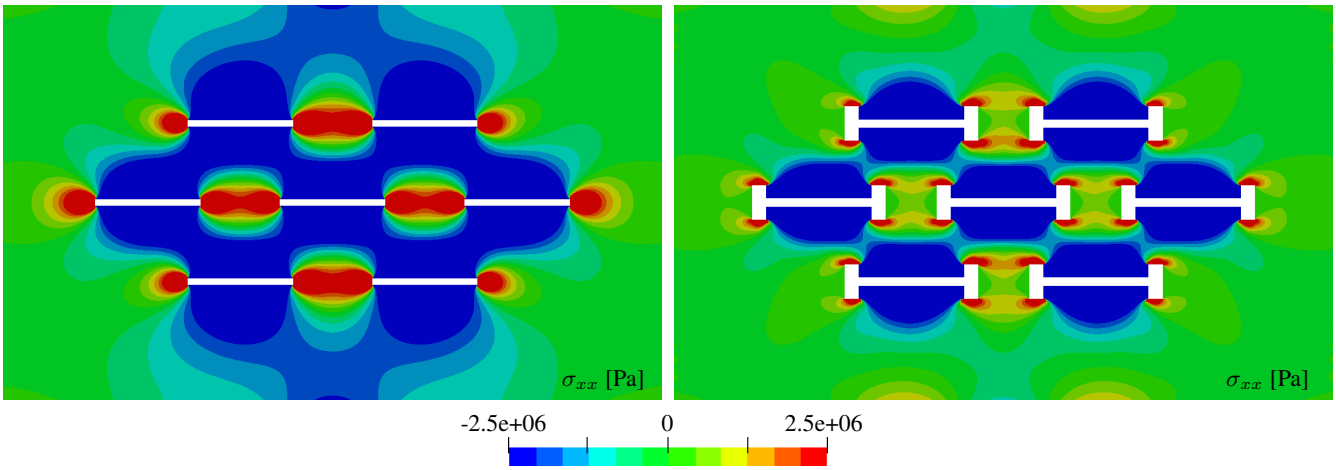

Fig. 7: Final state of stress inside the concrete domain for a regular multi-fiber arrangement. Simulations were performed in plane stress. Left: Standard fibers. Right: Improved fibers with anchors and elastomeric coating.

It shows that for both types of fibers, regions of compression unite. For straight fibers, in between the tips, this is also characteristic for tension. Noticeably, regions of compression are more pronounced for straight fibers. The presence of anchors kind of shields their propagation. Note that by using the elastomeric coating, the region of tension is shifted away from the tips towards the sides of the anchors and is reduced noticeably in its magnitude.

5 Conclusions and Outlook

The concept of creating a prestress state in concrete using shape memory alloys was proven to be applicable. However, for straight fibers, pronounced regions of tension will occur as well. Stresses in longitudinal direction of fibers are not greatly influenced by the strain release type, whereas radial and circumferential stresses are. By introducing tip anchors and an elastomeric coating in typical regions of tension, an almost pure state of compression can be created. Furthermore, the coating will thermally insulate fibers which is beneficial for efficacy of inductive heating. Generally, there are synergies regarding compression in multi-fiber configurations. For the improved fiber geometry, they were found to be weaker.

The next step could be to use a state-of-the-art material model. This requires simulating the process of pre-stretching, but might answer open questions regarding the strain release type. Furthermore, interactions between phase change and hindrance of fiber contraction by the concrete can be investigated. Regarding multi-fiber interaction, more dense and random configurations need to be investigated. For this purpose, techniques of handling non-conforming meshes, such as the mortar method, need to be applied. It would also enable to investigate 3D multi-fiber cases with reasonable effort. Those are vital to gain a profound understanding of interactions.

Acknowledgements Open access funding enabled and organized by Projekt DEAL.

References

[1] M. Schleiting, A. Wetzel, F. Gerland, T. Niendorf, O. Wünsch and B. Middendorf, RheoCon 2019, RILEM Books. **23**, 142-148 (2020)
[2] E. Fehling, M. Schmidt, J. Walraven, T. Leutbecher and S. Fröhlich, UHPC: Fundamentals, Design, Examples (Wiley, Berlin,2014)
[3] N. Banthia and J. F. Trottier, Cem Concr Res **9**, 158-168 (1991)
[4] D. Y. Yoo, H. K. Sohn, P. H. R. Borges and R. F. Soonho Kim, J Mater Res and Technol **9**, 2914-2925 (2020)
[5] M. Vollmer, A. Bauer, J.-M. Frenck, P. Krooß, A. Wetzel, B. Middendorf, E. Fehling and T. Niendorf, Eng Struct **241**, 112430 (2021)
[6] H. P. Heim, J. C. Zarges, K. Klier, B. Middendorf, A. Wetzel, M. Schleiting and N. Wiemer, German Patent **DE102020110643.2** (2020)
[7] N. Wiemer, A. Wetzel, M. Schleiting, P. Krooß, M. Vollmer, T. Niendorf, S. Böhm and B. Middendorf, Materials **13**, 3128 (2020)
[8] T. Niendorf, F. Brenne,P. Krooß, M. Vollmer, J. Günther, D. Schwarze and H. Biermann, Metall Mater Trans A **47**, 2569–2573 (2016)
[9] T. Gleim, D. Kuhl, M. Schleitling, A. Wetzel and B. Middendorf, PAMM **19**, e201900025 (2019)
[10] D. J. Hartl and D. C. Lagoudas, Proc Inst Mech Eng G J Aerosp Eng **221**, 535-552 (2007)

[11] J.A. Shaw, C.B. Churchill, and M.A. Iadicola, Exp Tech **32**, 55–62 (2008).
[12] K.M. Armattoe, C. Bouby, M. Haboussi and T. Ben Zineb, Int J Solids Struct **32**, 283-295 (2016)
[13] S. Descher and O. Wünsch, Arch Appl Mech Arch Appl Mech **92**, 1859–1878 (2022)
[14] T. Gleim and D. Kuhl, Arch Computat Methods Eng **26**, 405–447 (2019)
[15] T. Gleim, B. Schröder and D. Kuhl, Arch Appl Mech **85**, 1055–1073 (2015).
[16] T. Gleim, Simulation of Manufacturing Sequences of Functionally Graded Structures (Kassel University Press, 2016)
[17] V. Rudnev, D. Loveless, R. Cook and M. Black, Handbook of Induction Heating (Marcel Dekker, New York,2003)
[18] F. Gerland, T. Schomberg, D. Kuhl and O. Wünsch, PAMM **21**, 202100109 (2021)

